

Final-State Radiative Effects for the Exact  $\mathcal{O}(\alpha)$  YFS  
Exponentiated (Un)Stable  $W^+W^-$  Production  
At and Beyond LEP2 Energies<sup>†</sup>

S. Jadach<sup>a,b,c</sup>, W. Płaczek<sup>d,c</sup>, M. Skrzypek<sup>b,c</sup>, B.F.L. Ward<sup>e,f,c</sup> and Z. Was<sup>b,c</sup>

<sup>a</sup>*DESY, Theory Division, D-22603 Hamburg, Germany*

<sup>b</sup>*Institute of Nuclear Physics, ul. Kawiorów 26a, 30-055 Cracow, Poland,*

<sup>c</sup>*CERN, Theory Division, CH-1211 Geneva 23, Switzerland,*

<sup>d</sup>*Institute of Computer Science, Jagellonian University,  
ul. Nawojki 11, 30-072 Cracow, Poland,*

<sup>e</sup>*Department of Physics and Astronomy,  
The University of Tennessee, Knoxville, Tennessee 37996-1200, USA,*

<sup>f</sup>*SLAC, Stanford University, Stanford, California 94309, USA.*

**Abstract**

We present the leading-logarithm (LL) final-state radiative effects for the exact  $\mathcal{O}(\alpha)$  YFS exponentiated (un)stable  $WW$  pair production at LEP2/NLC energies using Monte Carlo event generator methods. The corresponding event generator, version 1.12 of the program YFSWW3, wherein both Standard Model and anomalous triple gauge-boson couplings are allowed, generates  $n(\gamma)$  radiation both from the initial state and from the intermediate  $W^+W^-$  state, and generates the LL final state  $W$  decay radiative effects. Sample Monte Carlo data are given for illustration.

*To be submitted to Physical Review D*

---

† Work partly supported by the Polish Government grants KBN 2P30225206 and 2P03B17210, the Maria Skłodowska-Curie Joint Fund II PAA/DOE-97-316, and by the US Department of Energy Contracts DE-FG05-91ER40627 and DE-AC03-76ER00515.

The role of the final-state radiative (FSR) effects in the processes  $e^+e^- \rightarrow W^+W^- + n(\gamma) \rightarrow 4f+n(\gamma)$  at and beyond LEP2 energies is of considerable interest for the LEP2 and NLC physics programs [1, 2, 3]. In this paper, we evaluate for the first time the possible interplay between the exact  $\mathcal{O}(\alpha)$  electroweak (EW) corrections and the leading-logarithm (LL) final-state radiative effects for these processes when the  $n(\gamma)$  radiation is realized according to the amplitude-based Monte Carlo event generator techniques described in Refs. [4, 5], wherein infrared singularities are cancelled to all orders in  $\alpha$  by using the extension to spin 1 charged particles of the theory of Yennie, Frautschi and Suura for QED [6].

The final-state radiative effects are realized in the LL approximation using the calculation of the program PHOTOS (Ref. [7]) in which a non-radiative final-state process is used to generate up to two photons in the corresponding radiative process by iterating the structure function evolution equation<sup>1</sup> for QED [8]. The exact  $\mathcal{O}(\alpha)$  YFS exponentiated final-state  $W$  decay radiative effects will be published elsewhere [9]. In this connection, we note that we expect the non-leading  $\mathcal{O}(\alpha)$  and higher order ( $\mathcal{O}(\alpha^n)$ ,  $n \geq 2$ ) final-state radiative effects to be small,  $\sim 1\%$  in the peak reduction effect [2] for example, even for a “bare trigger” acceptance for the outgoing final charged particles. This has been found by the authors of Ref. [2], who analysed the effects of final-state radiation in  $Z$  decay in the naive exponentiated (exact and LL)  $\mathcal{O}(\alpha)$  approximation and who estimated the corresponding size of the analogous effects in  $W$  decay, such as  $\sim 14\%$  for the total peak reduction effect. Indeed, more recently, the authors of Ref. [2] have made an independent cross check on their estimates of the FSR line-shape effects for  $e^+e^- \rightarrow W^+W^- \rightarrow 4f$  in Ref. [3]. There they present an exact  $\mathcal{O}(\alpha)$  calculation of the process in the double-pole approximation (DPA), wherein they retain in the pole expansion [10] of the complete  $e^+e^- \rightarrow 4f$  amplitude, only the terms containing the double pole in the S-matrix at the complex mass squared,  $M^2 = M_W^2 - iM_W\Gamma_W$ , where  $M_W, \Gamma_W$  are the respective mass and width of the  $W$  boson, and where in the residues of the respective double poles they project the respective  $\mathcal{O}(\alpha)$  corrections to an appropriate on-shell point. Henceforth, we refer to the on-shell residue projected DPA as to the leading pole approximation (LPA), with more general applications in mind: for example, in a triply resonant process, the LPA would correspond to the triple pole terms in the respective S-matrix element with the residues projected to an appropriate on-shell point. In this gauge-invariant calculation, these authors find that the FSR peak reduction effect is  $\sim 14.4\%$  for  $W^{+(-)} \rightarrow e^{+(-)}\nu_e(\bar{\nu}_e)$ , to be compared with their estimate of  $\sim 14\%$  in Ref. [2]. We will compare our results with those in Refs. [2, 3]. We emphasise that our work differs from the work of Ref. [2] in that we include the exact EW  $\mathcal{O}(\alpha)$  corrections with YFS exponentiation in the production process and we actually calculate the effects of the FSR in the  $W$ -pair production and decay process at LEP2/NLC energies; in Ref. [2], only the process  $\nu_\mu\bar{\nu}_\mu \rightarrow ZZ \rightarrow e^+e^- + \nu_\tau\bar{\nu}_\tau$  is actually calculated, and a heuristic argument is used to estimate the corresponding

---

<sup>1</sup>To be precise an ansatz is provided, which reproduces the LL terms. It includes transverse degrees of freedom for the photon 4-momentum, assures coverage of the full phase space and rules of energy-momentum conservation. The photons’ angular distribution is chosen to reproduce exactly the one of the soft photon limit. See Ref. [7] for more details.

results for final-state  $W$ -decay radiation. Thus, our calculations will also be a comment on the accuracy of these heuristic arguments in the presence of the YFS exponentiated exact  $\mathcal{O}(\alpha)$  corrections to the  $W$ -pair production process. Our work differs from that in Ref. [3] in that we include the YFS exponentiation of the exact  $\mathcal{O}(\alpha)$  production process in the  $W$ -pair intermediate state and the  $\mathcal{O}(\alpha)^2$  LL FSR whereas, in Ref. [3], the exact  $\mathcal{O}(\alpha)$  correction to the production and decay processes for the  $W$ -pair in the leading pole approximation is calculated without exponentiation. The leading pole approximation treatment of the attendant non-factorizable corrections in Refs. [11, 12, 14] is also retained. The latter non-factorizable corrections have been shown [11, 12, 14] to be small and, as we explain in Ref. [5], when one works up to but not including  $\mathcal{O}(\frac{\alpha}{\pi} \frac{\Gamma_W}{M_W})$  as we do, such effects may be dropped; which we do. Thus, although we start our calculation in Ref. [5] in the fermion-loop scheme [15], when we focus on the  $\mathcal{O}(\alpha)$  EW correction, we go to the leading pole part of the respective production amplitude. We also make the approximation of using on-shell residues for this double pole part, with which we then approximate the corresponding  $\mathcal{O}(\alpha)$  EW correction. In our Monte Carlo event generator approach, we stress that the full off-shell phase space is always retained here. We improve our result by using the complete on-shell residues for EW corrections rather than their on-shell fermion-loop scheme representatives. Indeed, for the QED bremsstrahlung correction we stress that, since the real photon has  $k^2 = 0$ , the corresponding running charge is the usual one. It can thus be shown that, in  $\mathcal{O}(\alpha)$ , bremsstrahlung residues of the on-shell fermion-loop scheme are equivalent to those in the LPA; in both cases all infrared singularities are properly cancelled and not only the QED gauge invariance is preserved but also the full  $SU_{2L} \times U_1$  gauge invariance [4, 5]. For this reason, in order  $\mathcal{O}(\alpha)$ , in our final result, any reference to the fermion-loop scheme is purely pedagogical. What we arrive at is precisely the LPA, with full on-shell residues for the respective double pole approximation. Indeed, as the YFS expansion is not generally familiar, if one looks at Eqs. (1) and (2) in Ref. [5], which give the on-shell  $\mathcal{O}(\alpha)$  contributions to the YFS residuals  $\bar{\beta}_0$  and  $\bar{\beta}_1$ , respectively, for the production process in the LPA, one may think that the lowest-order contribution to  $\bar{\beta}_0$ ,  $\bar{\beta}_0^{(0)}$  in the notation of Ref. [5], is *not* required either to be evaluated at the corresponding on-shell point as well. However, the right-hand side of Eq. (2) in Ref. [5], for example, involves the subtraction, from the corresponding on-shell  $\mathcal{O}(\alpha)$  bremsstrahlung cross section, of the product of the YFS real emission infrared function  $\bar{S}$  [6, 4] by the on-shell lowest order Born cross section; *we need to stress that the YFS theory then forces the contribution to  $\bar{\beta}_0$  corresponding to this respective lowest-order Born cross section,  $\bar{\beta}_0^{(0)}$ , to be evaluated at the on-shell point as well.* Thus, according to the YFS theory, Eqs. (1) and (2) in Ref. [5] are entirely equivalent to results in Refs. [3] for the production process, for the contributions up to and including terms  $\mathcal{O}(\alpha)$ . As can also be seen from the results in Refs. [3], these approximations are valid up to but not including  $\mathcal{O}(\frac{\alpha}{\pi} \frac{\Gamma_W}{M_W})$ . We then apply the YFS Monte Carlo methods of two of us (S.J. and B.F.L.W.) [16], as extended to spin 1 particles in Ref. [4], to arrive at the respective exact  $\mathcal{O}(\alpha)_{prod}$  YFS exponentiated results realized in YFSWW3-1.11. Hence, we stress that, as far as the  $\mathcal{O}(\alpha)$  correction to the production process under study is concerned, the results in Refs. [3, 5] should be equivalent, in view of the many cross checks carried out by the

authors of Refs. [17, 18, 19] on the two corresponding electroweak on-shell calculations used therein.

More precisely, starting from the calculations in the program YFSWW3-1.11 in Ref. [5], which feature the exact  $\mathcal{O}(\alpha)_{prod}$  YFS exponentiated results for the process  $e^+e^- \rightarrow W^+W^- + n(\gamma) \rightarrow 4f + n(\gamma)$ , we have interfaced the outgoing final state to the program PHOTOS [7]. The latter uses the structure function evolution equation for QED [8] to generate up to two final-state decay photons for each  $W$  according to the respective LL probabilities to radiate; here the corresponding angular distributions of the decay photons are all generated in accordance with this LL approximation as described in Ref. [7]. The net probability of the respective event is unchanged, i.e. the normalization of YFSWW3-1.11 is unaffected by this interface, which will be described in more detail elsewhere [9]. We refer to the version of YFSWW3 that contains this final-state radiative interface to PHOTOS as YFSWW3-1.12 and it is available from the authors [13]. In what follows, we present some sample Monte Carlo data from YFSWW3-1.12 to look into the possible role of FSR in the presence of the  $\mathcal{O}(\alpha)$  EW corrections. For definiteness, we focus here on the current LEP2 CMS energy of 190 GeV and on the SM couplings. The complete discussion of both LEP2 and NLC energies with the illustration of anomalous couplings will appear elsewhere [9].

Specifically, in Figs. 1–8, we show the results obtained with YFSWW3-1.12 on the processes  $e^+e^- \rightarrow W^+W^- + n(\gamma) \rightarrow \bar{c}s + \ell\bar{\nu}_\ell$ ,  $\ell = e, \mu$ , for the cosine of the  $W$  production angle distribution in the CM (LAB) system, for the  $W$  mass distribution, with both “bare” and “calorimetric” definitions of that mass, for the CMS lepton final energy distribution, for both calorimetric and bare definitions of that energy, and for the corresponding distributions of the cosine of the lepton decay angle in the  $W$  rest frame. We note the following properties of these results. First, concerning the  $W$  mass distributions in Figs. 1 and 5, we see that the respective average values of  $M_W$  are as given in Table 1. There, *EW-ex* denotes the exact  $\mathcal{O}(\alpha)_{prod}$  calculation of EW corrections [5]; *EW-ap* denotes the approximate treatment of these EW corrections as given in Ref. [20]; *No EW* denotes that the EW corrections other than the ones coming from LL ( $\mathcal{O}(\alpha^2)$ ) initial-state radiation are turned off. The calorimetric results are all closer to their respective *NO FSR* analogues than are the bare results, as expected. The effects of the FSR for the muon case are all respectively smaller than the corresponding results for the electron case, again as expected because of the smaller radiation probability for the muon. The size of the shift of  $\langle M_W \rangle$  is generally consistent with the discussion in Ref. [2], which deals with primarily the line shape (peak position and height); in detail we see that, in the presence of the FSR, at the level of our statistical errors, for an average quantity such as  $\langle M_W \rangle$ , all three calculations in the table are sufficient, as expected. With regard to the guesstimates made in Ref. [2] concerning the peak reduction and the peak position shift, we see from the *BARE* curves in Fig. 1 that our result of 13.5% for the peak reduction in the  $e^-$  case (comparing the *EW-ex* curves with and without FSR) is in good agreement with the 14% guesstimate of Ref. [2] and with the 14.4% found in the recent  $\mathcal{O}(\alpha)$  on-shell LPA results in Ref. [3]. The  $\sim -57$  MeV guesstimated in Ref. [2] for the corresponding peak position shift in the  $e^-$  case was recently updated to  $-77$  MeV in Ref. [3]; for the  $\mu$  case, the up-

$E_{CM}$ [GeV]	Calculation	FSR	CUT	$\langle M_W \rangle$ [GeV]
		$W^- \rightarrow e^- \bar{\nu}_e$		
190	<i>Born</i>	–	<i>BARE</i>	$80.253 \pm 0.008$
	<i>EW-ex</i>	<i>NO</i>	<i>BARE</i>	$80.146 \pm 0.036$
	<i>No EW</i>	<i>NO</i>	<i>BARE</i>	$80.142 \pm 0.036$
	<i>No EW</i>	<i>YES</i>	<i>BARE</i>	$78.614 \pm 0.035$
	<i>EW-ap</i>	<i>YES</i>	<i>BARE</i>	$78.613 \pm 0.035$
	<i>EW-ex</i>	<i>YES</i>	<i>BARE</i>	$78.618 \pm 0.035$
	<i>No EW</i>	<i>YES</i>	<i>CALO</i>	$79.727 \pm 0.036$
	<i>EW-ap</i>	<i>YES</i>	<i>CALO</i>	$79.725 \pm 0.036$
	<i>EW-ex</i>	<i>YES</i>	<i>CALO</i>	$79.731 \pm 0.036$
		$W^- \rightarrow \mu^- \bar{\nu}_\mu$		
190	<i>Born</i>	–	<i>BARE</i>	$80.253 \pm 0.008$
	<i>EW-ex</i>	<i>NO</i>	<i>BARE</i>	$80.146 \pm 0.036$
	<i>No EW</i>	<i>NO</i>	<i>BARE</i>	$80.142 \pm 0.036$
	<i>No EW</i>	<i>YES</i>	<i>BARE</i>	$79.374 \pm 0.036$
	<i>EW-ap</i>	<i>YES</i>	<i>BARE</i>	$79.373 \pm 0.036$
	<i>EW-ex</i>	<i>YES</i>	<i>BARE</i>	$79.378 \pm 0.036$
	<i>No EW</i>	<i>YES</i>	<i>CALO</i>	$79.725 \pm 0.036$
	<i>EW-ap</i>	<i>YES</i>	<i>CALO</i>	$79.724 \pm 0.036$
	<i>EW-ex</i>	<i>YES</i>	<i>CALO</i>	$79.730 \pm 0.036$

Table 1: The results of the  $125 \times 10^6$  statistics samples (weighted events) (except for *Born*, where the sample is  $540 \times 10^6$  of such events) from YFSWW3-1.12 for the average value of  $M_W$  as computed with the levels of radiative corrections as indicated for both bare and calorimetric treatments of the final lepton. See the text for more details.

dated expectation from Ref. [3] for the peak position shift is  $-39$  MeV. For completeness, we note that the size of the peak reduction effect in the  $\mu$  case has been found to be  $\sim 8\%$  in Ref. [3] whereas in Fig. 5 we find  $7.6\%$ , again showing good agreement between our results and those in Ref. [3]. Indeed, to compare our results for the peak position shift with those just cited from Ref. [3], we have performed Breit–Wigner fits to our line shapes in Figs. 1 and 5 with the values, both fixed and floating, of the  $W$  width. The results of our fits are shown in Table 2. For comparison, the fits are done for two different mass intervals, from 78 GeV to 82 GeV, and from 76 GeV to 84 GeV, to illustrate the role of the wings of the resonance in the fits. From these results we find that the *BARE* peak position shifts are estimated using the narrow fit range as  $80.168 - 80.240 = -72$  MeV and  $80.199 - 80.241 = -42$  MeV for the  $e$  and  $\mu$  cases, respectively. We also computed the shift in the average invariant mass  $\langle M_W \rangle$  of the  $W$  in the narrow range from 78 GeV to 82 GeV as another estimate of the peak position shift for the *BARE* trigger and we found  $-81.5 \pm 1.4$  MeV and  $-43.9 \pm 0.9$  MeV for the  $e$  and  $\mu$  cases, respectively. Thus, both sets of estimators of the peak position shifts are in reasonable agreement with the results given

$M_W$ or $M_W/\Gamma_W$ [GeV]							
$W^- \rightarrow e^- \bar{\nu}_e$							
	$M$ -range [GeV]	<i>No FSR</i>		<i>FSR-BARE</i>		<i>FSR-CALO</i>	
		$\Gamma_W$ -fix	$\Gamma_W$ -fit	$\Gamma_W$ -fix	$\Gamma_W$ -fit	$\Gamma_W$ -fix	$\Gamma_W$ -fit
<i>Born</i>	78 – 82	80.240	80.240/2.0413				
	76 – 84	80.239	80.239/2.0376				
<i>No EW</i>	78 – 82	80.231	80.231/2.0442	80.166	80.168/2.2105	80.216	80.217/2.0831
	76 – 84	80.227	80.227/2.0372	80.142	80.135/2.2547	80.207	80.207/2.0892
<i>EW-ap</i>	78 – 82			80.166	80.168/2.2105	80.216	80.217/2.0832
	76 – 84			80.142	80.134/2.2547	80.207	80.207/2.0892
<i>EW-ex</i>	78 – 82	80.231	80.231/2.0443	80.166	80.168/2.2105	80.216	80.217/2.0832
	76 – 84	80.227	80.227/2.0372	80.142	80.134/2.2547	80.207	80.207/2.0892
$W^- \rightarrow \mu^- \bar{\nu}_\mu$							
<i>Born</i>	78 – 82	80.241	80.241/2.0308				
	76 – 84	80.250	80.250/2.0295				
<i>No EW</i>	78 – 82	80.232	80.232/2.0342	80.198	80.199/2.1196	80.217	80.218/2.0731
	76 – 84	80.238	80.238/2.0307	80.192	80.190/2.1481	80.217	80.217/2.0845
<i>EW-ap</i>	78 – 82			80.198	80.199/2.1196	80.217	80.218/2.0731
	76 – 84			80.192	80.190/2.1481	80.217	80.217/2.0845
<i>EW-ex</i>	78 – 82	80.232	80.232/2.0343	80.198	80.199/2.1196	80.217	80.218/2.0731
	76 – 84	80.238	80.238/2.0307	80.192	80.190/2.1481	80.217	80.217/2.0845

Table 2: The results of the Breit–Wigner line shape fit to the YFSWW3-1.12 MC sample for the  $W^-$  invariant mass distribution at  $E_{CMS} = 190$  GeV. The input values of the  $W$  mass and width were:  $M_W = 80.23$  GeV and  $\Gamma_W = 2.03367033$  GeV (this value was used in the  $\Gamma_W$ -fix fit). The fits were performed for two  $W$  invariant mass  $M$  ranges – as indicated in the table. See the text for more details.

in Ref. [3]<sup>2</sup>; in this connection, we recall the slight difference in beam energy between our studies (95 GeV) and those in Ref. [3] (92 GeV). Moreover, we see in Table 2 the same pattern of results as we see in Table 1: the FSR effects for the  $e$  case are more pronounced than those for the  $\mu$  case; the calorimetric acceptance reduces the size of the FSR effects; the results are not very sensitive to the EW correction to the production process. If we compare the predictions with and without FSR for the *EW-ex* and *no EW* cases we get a measure of the modulation of the FSR on the EW correction. From the curves in our Figs. 1 and 5 and the respective plots of the  $\delta_{RAD}$  as defined in the figures we see that this modulation is as expected. Concerning the cosine of the  $W$  production angle distributions, we see the interplay of the exact EW corrections on the one hand and the FSR on the other. Further, we see that the approximate EW corrections of Ref. [20], while a definite improvement over the no EW corrections at all, are not sufficient to describe this interplay at the level of 0.5–1.0%. Similar remarks hold for the lepton energy distribution in the CM system, although the corresponding insufficiency is reduced to the level of  $\sim 0.3\%$  for the *BARE* case, for example for electrons. Concerning the distributions of the cosine

<sup>2</sup> The fit mass shift and the peak position shift approach one another as the fit range approaches a zero size interval around the peak; a similar remark applies to the shift in the average mass relative to the range over which it is taken around the peak.

of the lepton decay angle in the  $W$  rest frame, we again see the importance of including both the EW corrections and the FSR in Figs. 4 and 8, for the electron and the muon, respectively. In all cases, the results for the muon, particularly the *BARE* results, are less affected by the FSR than are the corresponding results for the electron, as expected. We stress that our results in Figs. 1–8 are generally consistent with those in Ref. [3] keeping in mind that we treat the  $\mathcal{O}(\alpha^2)$  LL FSR and the YFS exponentiated on-shell exact  $\mathcal{O}(\alpha)_{prod}$  production process, whereas Ref. [3] treats only  $\mathcal{O}(\alpha)$  corrections in our LPA, in which only on-shell residues are used. Indeed, in addition to the agreements already cited, we call the reader’s attention to the normalization correction in Fig. 9 of Ref. [3]: at the CMS energy of  $\sqrt{s} = 190$  GeV, it is  $-11\%$ , in very good agreement with our result in Ref. [5], which is  $(1 + \delta_{prod})(\rho_w)^2 - 1 \cong -11.1\%$ , for the latter result, we have used Table 2 in Ref. [5] for the relative correction  $\delta_{prod} = -9.9\%$  to the production process, and the result in Ref. [21] for the  $\mathcal{O}(\alpha)$  correction to the leptonic partial width  $\rho_w - 1 \cong -0.686\%$ . In addition, we can note that, for the case of the  $\tau\bar{\nu}_\tau$  decay channel, our results are also consistent with those in Ref. [3] for the peak position shift and peak reduction effects. In view of our higher-order corrections, we find quite reasonable all the agreements noted here. A more detailed discussion of such comparisons will appear [9]. We stress that we have arrived at our results through a MC event generator realization of our calculation, in which realistic, finite  $p_T$ ,  $n(\gamma)$  radiation is incorporated in the production process on an event-by-event basis, whereas the results in Ref. [3] are all semi-analytical. This enhances the significance of the general agreement of our results where they do overlap.

The issue of whether the calorimetric results are more realistic than the bare ones appears to depend on whether one is talking about the muon or the electron<sup>3</sup>. For the electron, it is very difficult to separate the soft photons with energy  $\lesssim \Gamma_W$  that are responsible for the FSR effects of the  $W$  line shape as discussed already in Refs. [2, 3]; they are just a part of the electromagnetic calorimeter response in general, which is used to measure the electron energy. For the muon, the energy is usually measured by a muon chamber in which, in general, these soft photons are not present. Thus, for the electron, our calorimetric results are more realistic; for the muon, it is the other way around. In either case, we see that precision  $W$ -pair production and decay studies need to take the interplay between the FSR and the EW corrections into account so as to obtain the most precise tests of the SM; our calculations in YFSWW3-1.12 offer an avenue to achieve that goal.

## Acknowledgements

Two of us (S.J. and B.F.L.W.) acknowledge the kind hospitality of Prof. A. De Rújula and the CERN Theory Division while this work was being completed. Two of us (B.F.L.W. and W.P.) acknowledge the support of Prof. D. Schlatter and the ALEPH Collaboration in the final stages of this work. One of us (Z.W.) acknowledges the support of the L3 group of ETH Zurich during the time this work was performed.

---

<sup>3</sup>T. Kawamoto, private communication, 1998.

## References

- [1] W. Beenakker et al., *WW Cross-Sections and Distributions*, in *Physics at LEP2*, edited by G. Altarelli, T. Sjöstrand and F. Zwirner (CERN 96-01, Geneva, 1996), Vol. 1, p. 79.
- [2] W. Beenakker, F. A. Berends and A. P. Chapovsky, preprint hep-ph/9805327, 1998; Phys. Lett. **B435** (1998) 233.
- [3] W. Beenakker, F. A. Berends and A. P. Chapovsky, preprint hep-ph/9811481, 1998; preprint hep-ph/9902333, 1999.
- [4] S. Jadach, W. Płaczek, M. Skrzypek and B.F.L. Ward, Phys. Rev. **D54** (1996) 5434.
- [5] S. Jadach, W. Płaczek, M. Skrzypek, B.F.L. Ward and Z. Wąs, Phys. Lett. **B417** (1998) 326.
- [6] D. R. Yennie, S. Frautschi and H. Suura, Ann. Phys. **13** (1961) 379.
- [7] E. Barberio and Z. Wąs, Comput. Phys. Commun. **79** (1994) 291 and references therein.
- [8] See for example, G. Altarelli and G. Martinelli, in *Physics at LEP*, eds. J. Ellis and R. Peccei (CERN 86-02, Geneva, 1986), Vol. 1, p. 47; and references therein.
- [9] S. Jadach et al., to appear.
- [10] R. G. Stuart, Phys. Lett. **B262** (1991) 113;  
A. Aeppli, G.J. van Oldenborgh and D. Wyler, Nucl. Phys. **B428** (1994) 126.
- [11] K. Melnikov and O. Yakovlev, Nucl. Phys. **B471** (1996) 90.
- [12] W. Beenakker, F. A. Berends and A. P. Chapovsky, Phys. Lett. **B411** (1997) 203; Nucl. Phys. **B508** (1997) 17.
- [13] S. Jadach et al., *YFSWW3 1.12 MC Event Generator*, available from the authors at the WWW URL <http://enigma.phys.utk.edu/pub/YFSWW>.
- [14] A. Denner, S. Dittmaier and M. Roth, Nucl. Phys. **B519** (1998) 39; Phys. Lett. **B429** (1998) 145.
- [15] U. Baur and D. Zeppenfeld, Phys. Rev. Lett. **75** (1995) 1002;  
W. Beenakker *et al.*, Nucl. Phys. **B500** (1997) 255 and references therein.
- [16] S. Jadach and B.F.L. Ward, Phys. Rev. **D38** (1988) 2897 and **40** (1989) 3582; Comput. Phys. Commun. **56** (1990) 351.



- [17] J. Fleischer, F. Jegerlehner and M. Zrałek, Z. Phys. **C42** (1989) 409;  
M. Zrałek and K. Kołodziej, Phys. Rev. **D43** (1991) 43;  
J. Fleischer, K. Kołodziej and F. Jegerlehner, Phys. Rev. **D47** (1993) 830;  
J. Fleischer *et al.*, Comput. Phys. Commun. **85** (1995) 29 and references therein.
- [18] M. Böhm *et al.*, Nucl. Phys. **B304** (1988) 463.
- [19] W. Beenakker *et al.*, Phys. Lett. **B258** (1991) 469; Nucl. Phys. **B367** (1991) 287.
- [20] S. Dittmaier, M. Böhm and A. Denner, Nucl. Phys. **B376** (1992) 29 and **B391** (1993) 483 (E).
- [21] D. Yu. Bardin, S. Riemann and T. Riemann, Z. Phys. **C32** (1986) 121 and references therein.

$$W^- \longrightarrow e^- \bar{\nu}_e$$

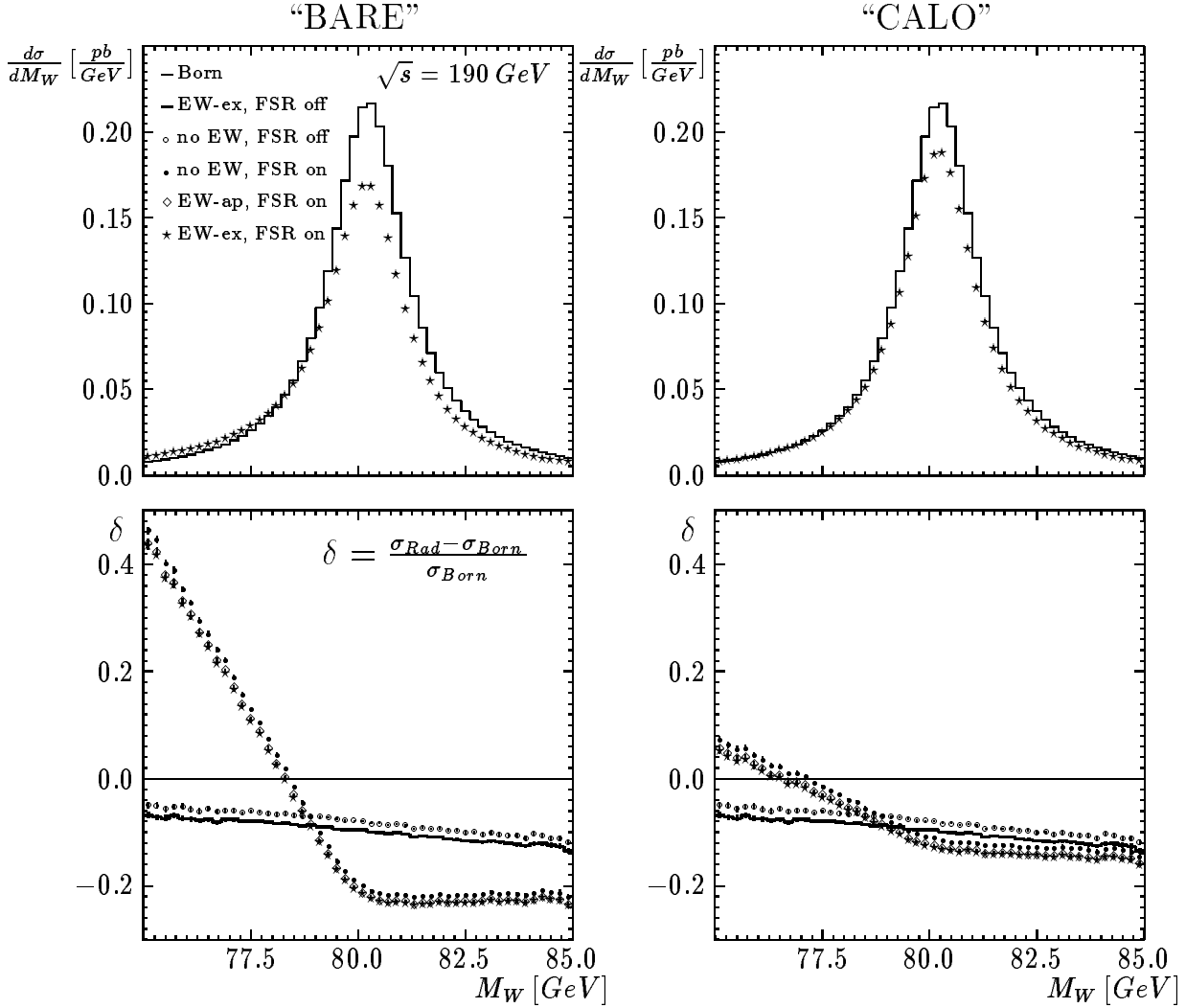


Figure 1: The invariant mass distributions of  $W^-$  reconstructed from its decay products,  $e^- \bar{\nu}_e$ , four-momenta. In the left pictures the electron is treated exclusively (‘bare’ electron), while in the right pictures it is treated calorimetrically (‘dressed’ electron – its four-momentum is combined with four-momenta of all photons emitted within an angle of  $5^\circ$  around its direction). The input values are  $M_W = 80.23 \text{ GeV}$ ,  $\Gamma_W = 2.034 \text{ GeV}$ .

$$W^- \longrightarrow e^- \bar{\nu}_e$$

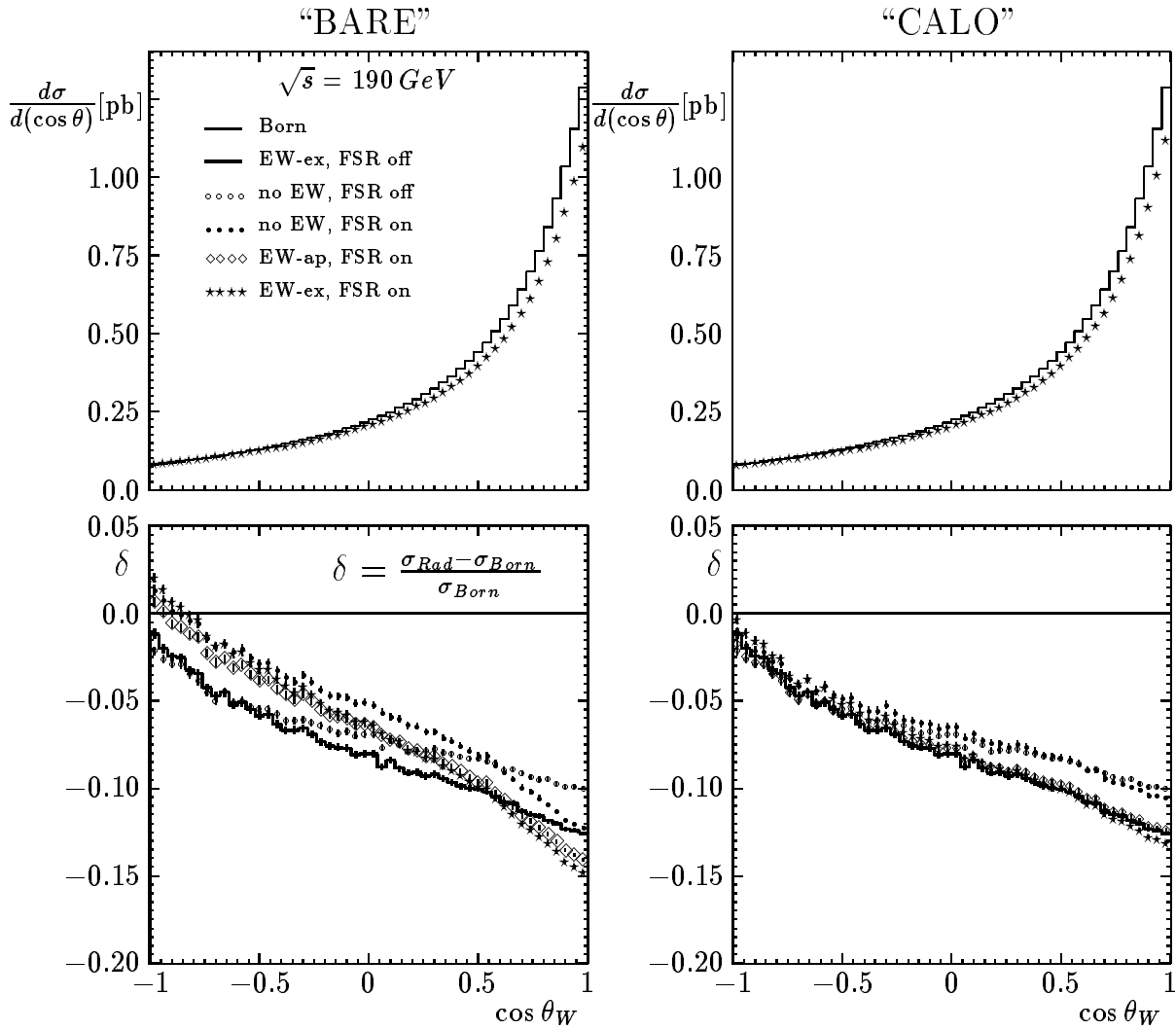


Figure 2: The angular distributions of  $W^-$  reconstructed from its decay products,  $e^- \bar{\nu}_e$ , four-momenta. In the left pictures the electron is treated exclusively ('bare' electron), while in the right pictures it is treated calorimetrically as defined in Fig. 1.

$$W^- \longrightarrow e^- \bar{\nu}_e$$

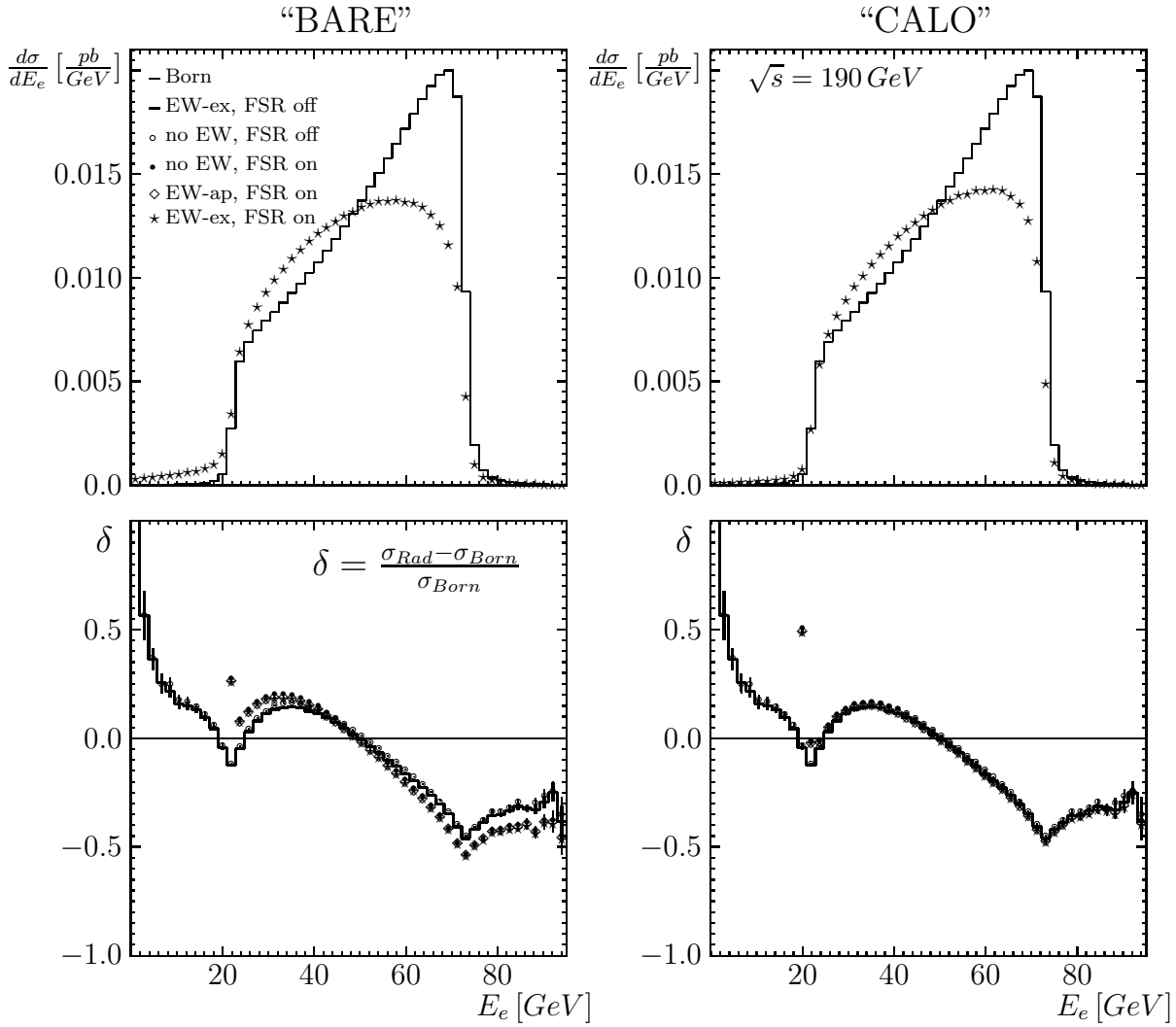


Figure 3: The distributions of the final state electron energy in the LAB frame. In the left pictures the electron is treated exclusively ('bare' electron), while in the right pictures it is treated calorimetrically as defined in Fig. 1.

$$W^- \longrightarrow e^- \bar{\nu}_e$$

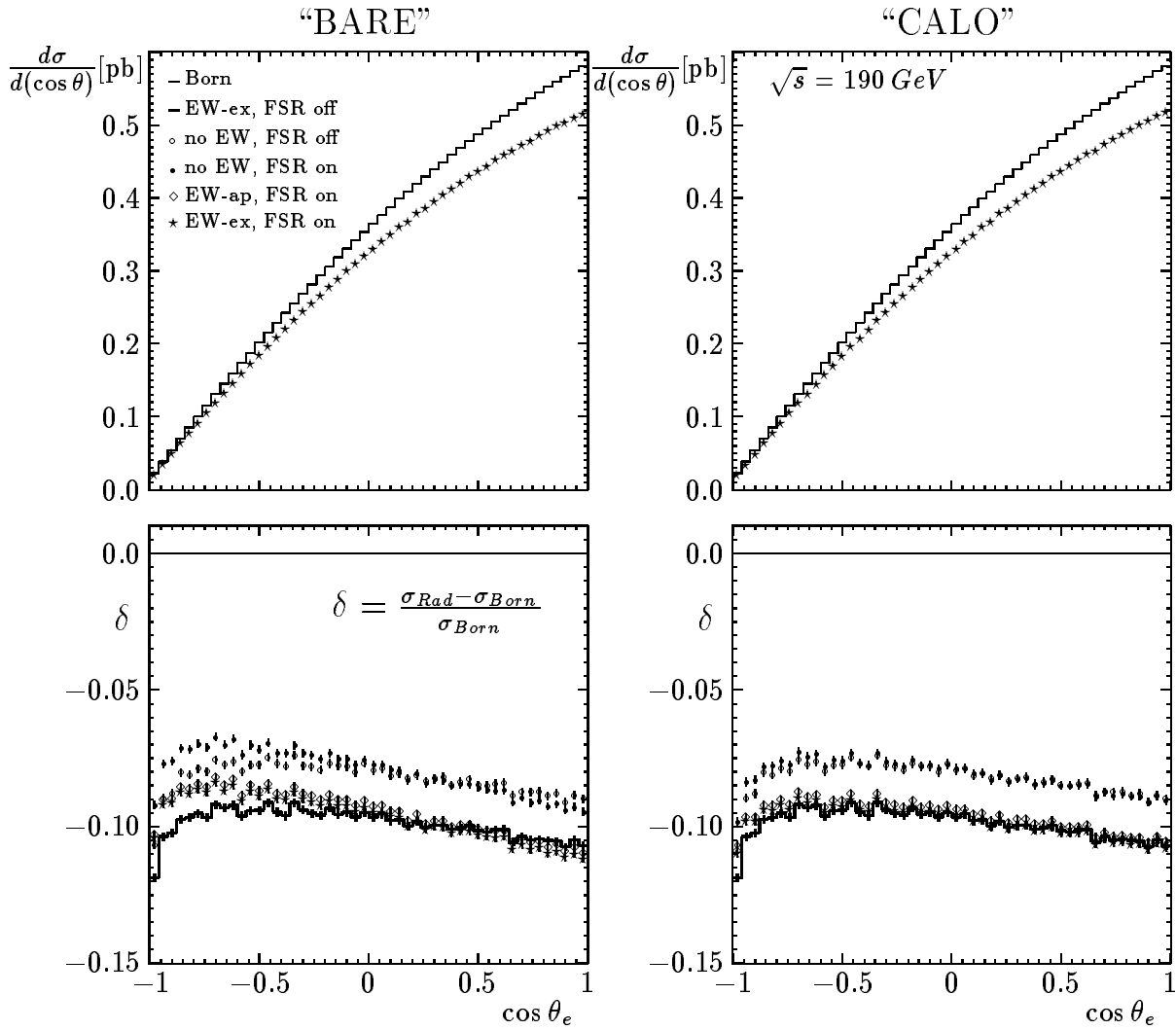


Figure 4: The distributions of the electron decay angle's cosine in the  $W^-$  rest frame. In the left pictures the electron is treated exclusively ('bare' electron), while in the right pictures it is treated calorimetrically as defined in Fig. 1.

$$W^- \longrightarrow \mu^- \bar{\nu}_\mu$$

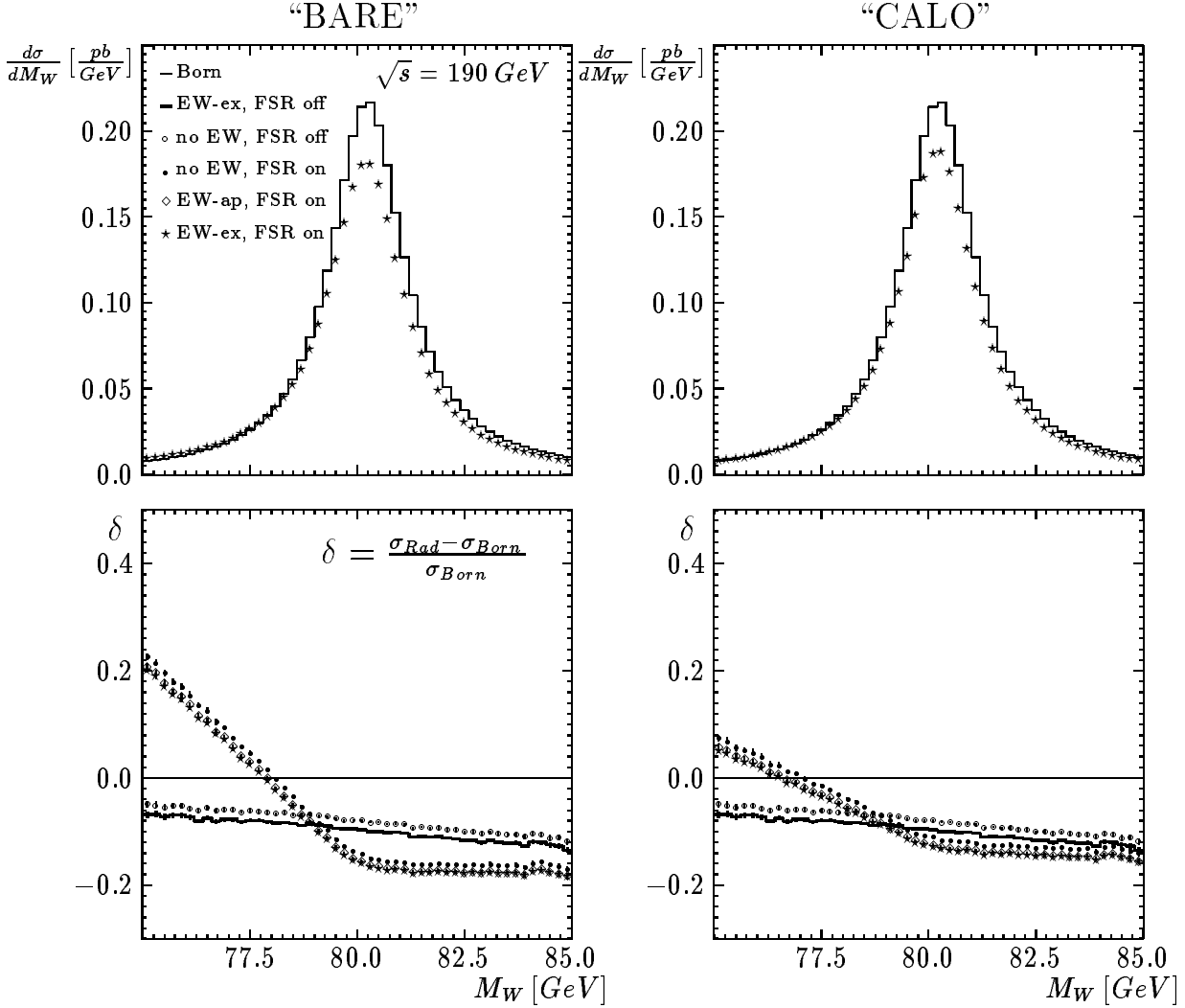


Figure 5: The invariant mass distributions of  $W^-$  reconstructed from its decay products,  $\mu^- \bar{\nu}_\mu$ , four-momenta. In the left pictures the muon is treated exclusively ('bare' muon), while in the right pictures it is treated calorimetrically as defined in Fig. 1. The input values are  $M_W = 80.23$  GeV,  $\Gamma_W = 2.034$  GeV.

$$W^- \longrightarrow \mu^- \bar{\nu}_\mu$$

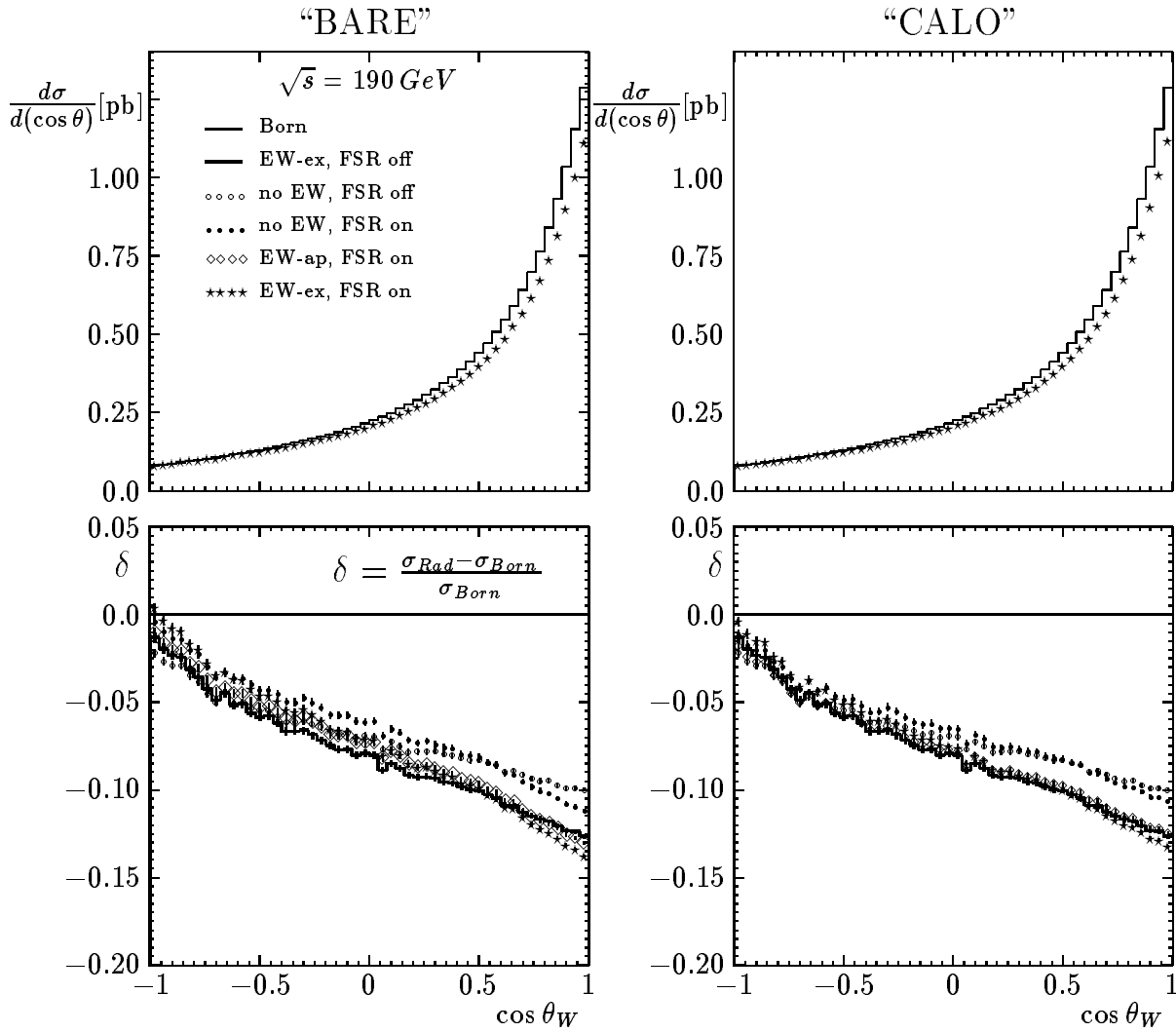


Figure 6: The angular distributions of  $W^-$  reconstructed from its decay products,  $\mu^- \bar{\nu}_\mu$ , four-momenta. In the left pictures the muon is treated exclusively ('bare' muon), while in the right pictures it is treated calorimetrically as defined in Fig. 1.

$$W^- \longrightarrow \mu^- \bar{\nu}_\mu$$

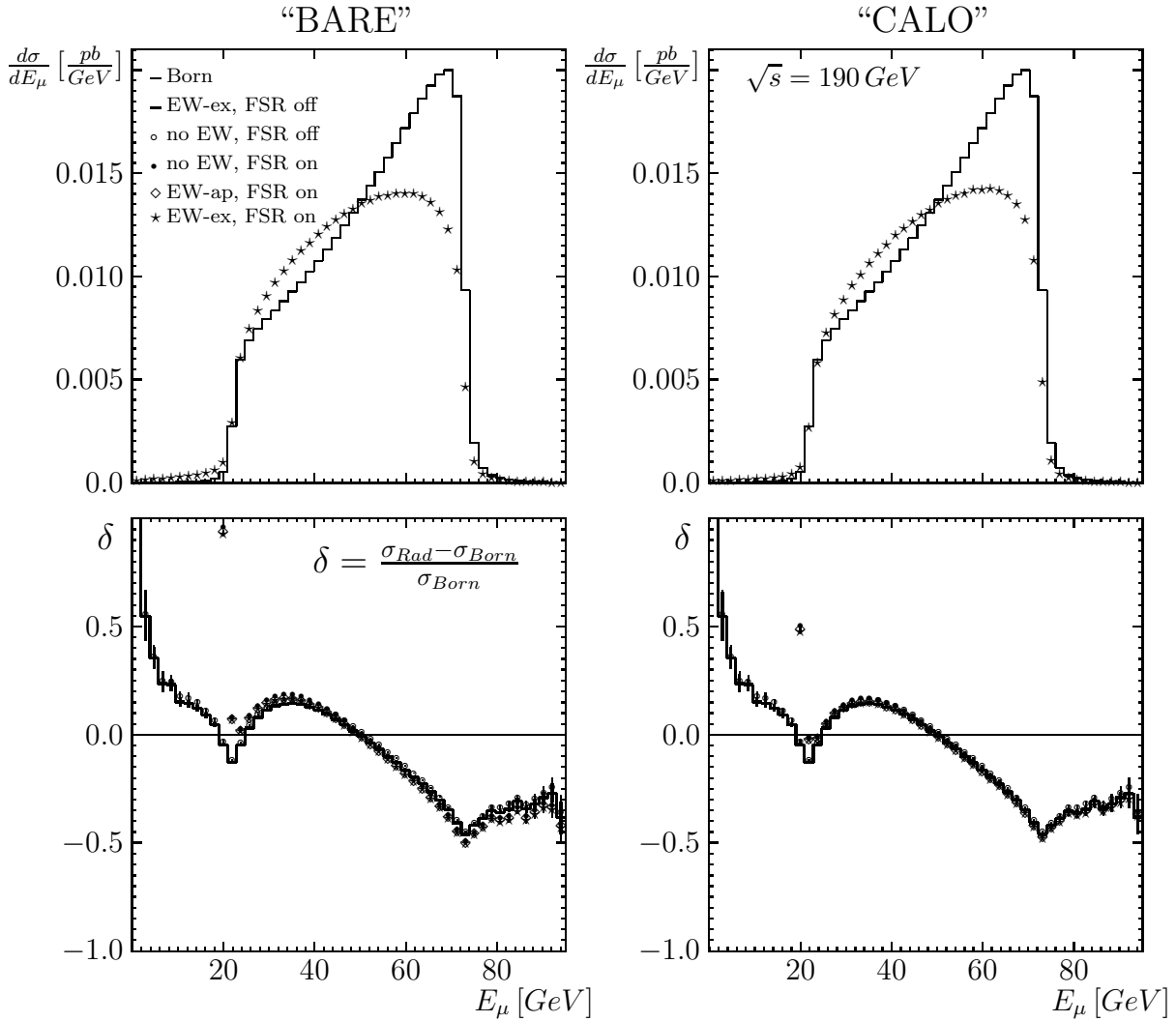


Figure 7: The distributions of the final state muon energy in the LAB frame. In the left pictures the muon is treated exclusively ('bare' muon), while in the right pictures it is treated calorimetrically as defined in Fig. 1.



$$W^- \longrightarrow \mu^- \bar{\nu}_\mu$$

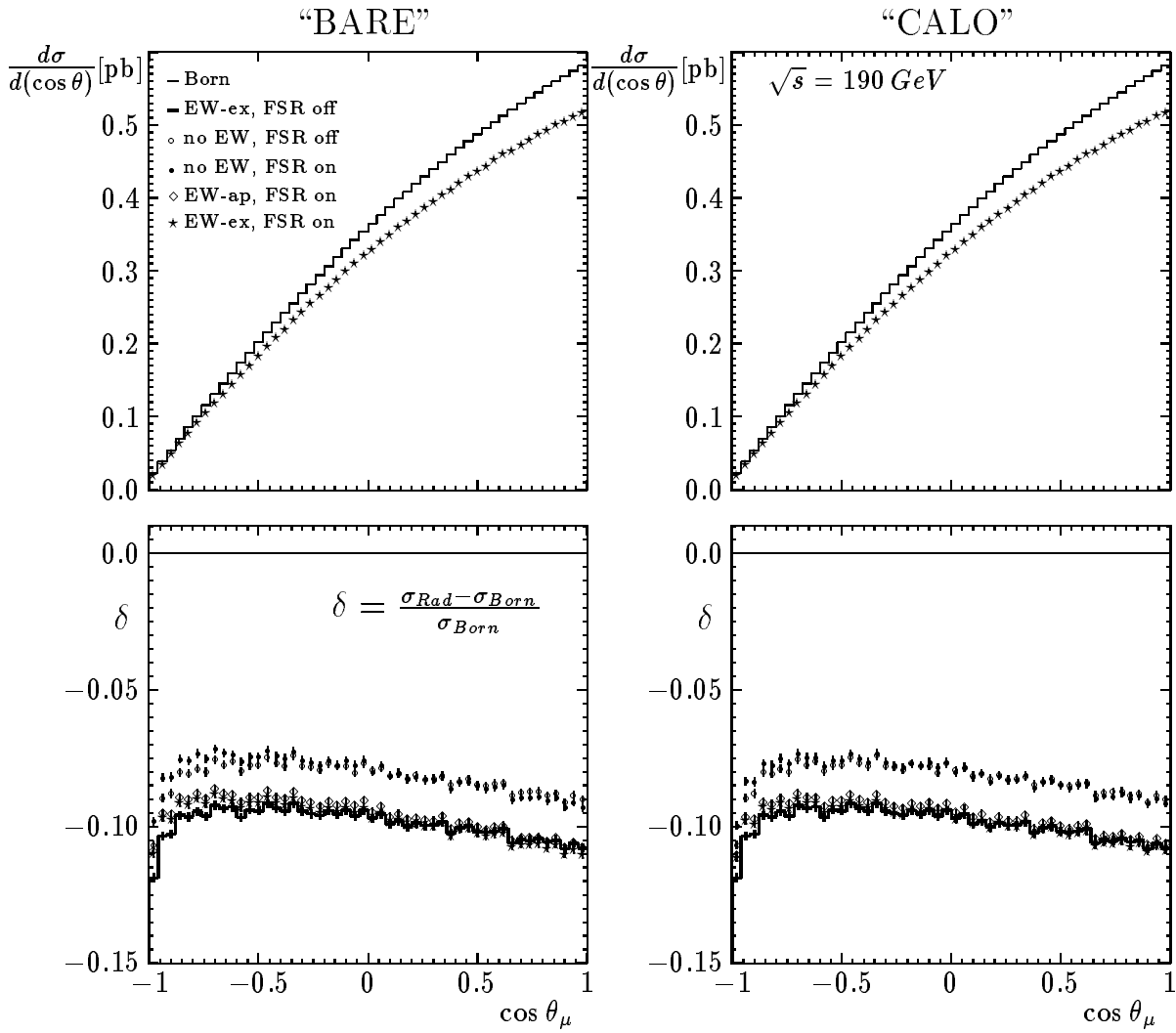


Figure 8: The distributions of the muon decay angle's cosine in the  $W^-$  rest frame. In the left pictures the muon is treated exclusively ('bare' muon), while in the right pictures it is treated calorimetrically as defined in Fig. 1.